Molecular Therapy
Original Article

Non-invasive administration of AAV to target lung parenchymal cells and develop SARS-CoV-2-susceptible mice

Myeon-Sik Yang,[1,8] Min-Jung Park,[2,3,8] Junhyeong Lee,[2,3,8] Byungkwan Oh,[1] Kyung Won Kang,[4] Yeonhwa Kim,[5] Sang-Myeong Lee,[5] Je-Oh Lim,[3] Tae-Yang Jung,[3] Jong-Hwan Park,[3,6] Seok-Chan Park,[1] Yun-Sook Lim,[7] Soon B. Hwang,[7] Kwang-Soo Lyoo,[7] Dong-il Kim,[2,3] and Bumseok Kim[1,7]

[1]Biosafety Research Institute and Laboratory of Veterinary Pathology, College of Veterinary Medicine, Jeonbuk National University, Iksan 54596, Korea; [2]Department of Veterinary Physiology, College of Veterinary Medicine, Chonnam National University, Gwangju 61186, Korea; [3]College of Veterinary Medicine and BK21 FOUR Program, Chonnam National University, Gwangju 61186, Korea; [4]Division of Biotechnology, College of Environmental and Bioresources, Jeonbuk National University, Iksan 54596, Korea; [5]College of Veterinary Medicine, Chungbuk National University, Cheongju 28644, Korea; [6]Laboratory Animal Medicine, College of Veterinary Medicine, Chonnam National University, Gwangju 61186, Korea; [7]Korea Zoonosis Research Institute, Jeonbuk National University, Iksan 54531, Korea

Adeno-associated virus (AAV)-mediated gene delivery holds great promise for gene therapy. However, the non-invasive delivery of AAV for lung tissues has not been adequately established. Here, we revealed that the intratracheal administration of an appropriate amount of AAV2/8 predominantly targets lung tissue. AAV-mediated gene delivery that we used in this study induced the expression of the desired protein in lung parenchymal cells, including alveolar type II cells. We harnessed the technique to develop severe acute respiratory syndrome coronavirus 2 (SARS-CoV-2)-susceptible mice. Three kinds of immune function-relevant gene knockout (KO) mice were transduced with AAV encoding human angiotensin-converting enzyme 2 (hACE2) and then injected with SARS-CoV-2. Among these mice, type I interferon receptor (IFNAR) KO mice showed increased viral titer in the lungs compared to that in the other KO mice. Moreover, nucleocapsid protein of SARS-CoV-2 and multiple lesions in the trachea and lung were observed in AAV-hACE2-transduced, SARS-CoV-2-infected IFNAR KO mice, indicating the involvement of type I interferon signaling in the protection of SARS-CoV-2. In this study, we demonstrate the ease and rapidness of the intratracheal administration of AAV for targeting lung tissue in mice, and this can be used to study diverse pulmonary diseases.

INTRODUCTION

Adeno-associated virus (AAV)-mediated gene delivery is promising for the treatment of human diseases as it triggers only a mild immune response, integrates into the host genome with a very low frequency, and can effectively infect human tissues.[1] Consequently, three AAV-based gene therapy drugs, namely Glybera, Luxturna, and Zolgensma, have been approved for clinical use, and dozens of drugs are being investigated under clinical trials.[2]

One of the benefits of using AAV vectors for gene therapy is that each of its serotypes shows tropism for different tissues and/or cell types.[3] For example, AAV2 infects kidneys, while AAV8 infects the pancreas. However, AAV2 and AAV8 also infect the liver, muscle, brain, and retina. To increase the targeting specificity and transduction efficacy, hybrid AAV vectors, such as AAV2/8 with a genome of serotype 2 and capsid protein of serotype 8, have been developed.[4,5] Although it is anticipated that AAV vectors should be tissue specific, selective targeting of lung parenchyma has not been achieved.[3]

Lungs are a part of the lower respiratory system, which is responsible for the exchange of gases in the body. The lung parenchyma consists of a large number of alveoli composed of multiple types of cells, including the alveolar epithelial cells, vascular endothelial cells, fibroblast, and pericytes.[6] Among these, alveolar epithelial cells are the most important cell type for maintaining the alveolar-capillary barrier function of the lungs. Alveolar epithelium is composed of alveolar type I (AT1) cells and alveolar type II (AT2) cells. AT1 cells are squamous cells that cover 95% alveolar surface and provide the surface area for gas exchange.[7] In contrast, AT2 cells are cuboidal cells and secrete the surfactant required to reduce the surface tension for preventing alveolar collapse.[8] In addition, AT2 cells serve as alveolar stem cells that can differentiate into AT1 cells, suggesting the pivotal role of AT1 and AT2 cells in lung homeostasis.[9]

Received 22 July 2021; accepted 5 January 2022;
https://doi.org/10.1016/j.ymthe.2022.01.010.

[8]These authors contributed equally

Correspondence: Dong-il Kim, Department of Veterinary Physiology, College of Veterinary Medicine, Chonnam National University, Gwangju 61186, Korea.
E-mail: kimdi@chonnam.ac.kr
Correspondence: Bumseok Kim, Biosafety Research Institute and Laboratory of Pathology, College of Veterinary Medicine, Jeonbuk National University, Iksan, 54596, Korea.
E-mail: bskims@jbnu.ac.kr

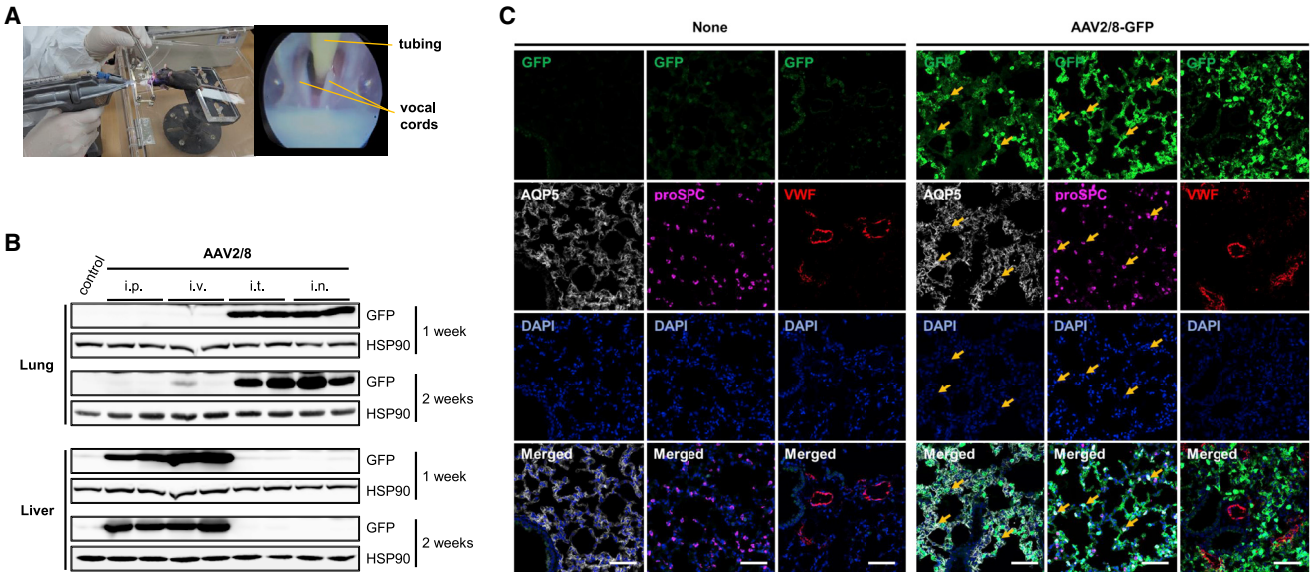

Figure 1. Intratracheal administration of AAV2/8 successfully targets lung parenchyma

(A) Instillator with an automatic video system allows for virus delivery over the epiglottis and vocal cords of the mice. (B) AAV2/8 encoding green fluorescent protein (GFP) or phosphate-buffered saline (PBS) was administered by intraperitoneal (i.p.), intravenous (i.v.), intratracheal (i.t.), or intranasal (i.n.) injection, followed by sacrificing the mice at 1 or 2 weeks post-injection. GFP expression in the lungs or livers was analyzed. HSP90 was used as the loading control. (C) Immunofluorescence analysis of the lungs of mice injected with PBS or with AAV2/8-GFP i.t. Signals for GFP, Aquaporin5 (AQP5), prosurfactant protein-C (proSPC), and von Willebrand factor (VWF), which are markers for AT1, AT2, or endothelial cells, respectively, are shown in green, white, pink, and red, respectively. DAPI stain used for nuclear staining appears blue. Arrows show representatively colocalized signals. Scale bar, 50 μm.

Severe acute respiratory syndrome coronavirus 2 (SARS-CoV-2) is the causative agent of the current coronavirus disease 2019 pandemic, and to combat it, an unprecedented number of studies are being conducted to better understand SARS-CoV-2. The SARS-CoV-2 genome is known to share 79% homology with SARS-CoV, which emerged in the Guangdong Province, southern China in 2002, and SARS-CoV-2, like SARS-CoV, uses the human angiotensin-converting enzyme 2 (hACE2) as a receptor to trigger cell entry.[10–12] However, one of the obstacles in SARS-CoV-2 research is that mice are not susceptible to SARS-CoV-2, since murine ACE2 does not support the binding to SARS-CoV-2.[13] The Perlman group developed hACE2 transgenic mice that are susceptible to SARS-CoV in 2007.[14] Despite the numerous advantages of using transgenic mice in terms of convenience and economic efficiency, it takes a long time to build a cohort and/or adopt hACE2 to mice with a different transgenic background.

In the present study, we found that non-invasive intratracheal administration of AAV specifically infects lung parenchymal cells, including AT2 cells. With this system, we generated an animal model that shows lung-specific hACE2 expression and is susceptible to SARS-CoV-2 using mice with different types of immune function-relevant gene knockouts (KOs).

RESULTS

Intratracheal administration of AAV2/8 specifically targets lung parenchyma

For the non-invasive intratracheal administration of AAV, we used the automatic video instillator, which facilitates the direct administration of AAV over the epiglottis and vocal cords, with an attached micro-camera (Figure 1A). To determine the effectiveness of the gene delivery to the pulmonary region, we generated the AAV2/8- or AAV2/9-expressing green fluorescent protein (GFP). We found that intratracheal delivery led to the successful expression of GFP in the lung, while this was not seen with intraperitoneal injection (Figure S1A). Expression levels of GFP were slightly higher in mice injected with AAV2/8 than in those injected with AAV2/9 (Figure S1A). Collectively, our results suggest that intratracheal delivery of the AAV vector, particularly AAV2/8, elicits expression of the desired protein in the lung tissue.

To further test the efficacy of injection routes for pulmonary-specific expression, 4×10^{11} viral particles (VPs) of AAV diluted in phosphate-buffered saline (PBS) was administered either intraperitoneally (500 μL), intravenously (50 μL), intratracheally (25 μL), or intranasally (25 μL), followed by the evaluation of GFP expression in lung tissue. GFP expression was predominant in the lung tissue of mice administered AAV either intratracheally or intranasally, while both intraperitoneal and intravenous injection of AAV led to exclusively high expressions of GFP in the liver (Figure 1B). GFP expression was not detected in the other tissues, such as the heart, brain, and kidneys (Figure S1B). We also intranasally and intratracheally administered higher doses and volumes of AAV. We found that the administration of 50 μL of 2×10^{12} VPs of AAV led to desirable GFP expression in the lung, but that it also led to higher expression of GFP in the liver, implying that a higher amount of virus injected was sufficient to reach the liver via systemic circulation (Figure S1C).

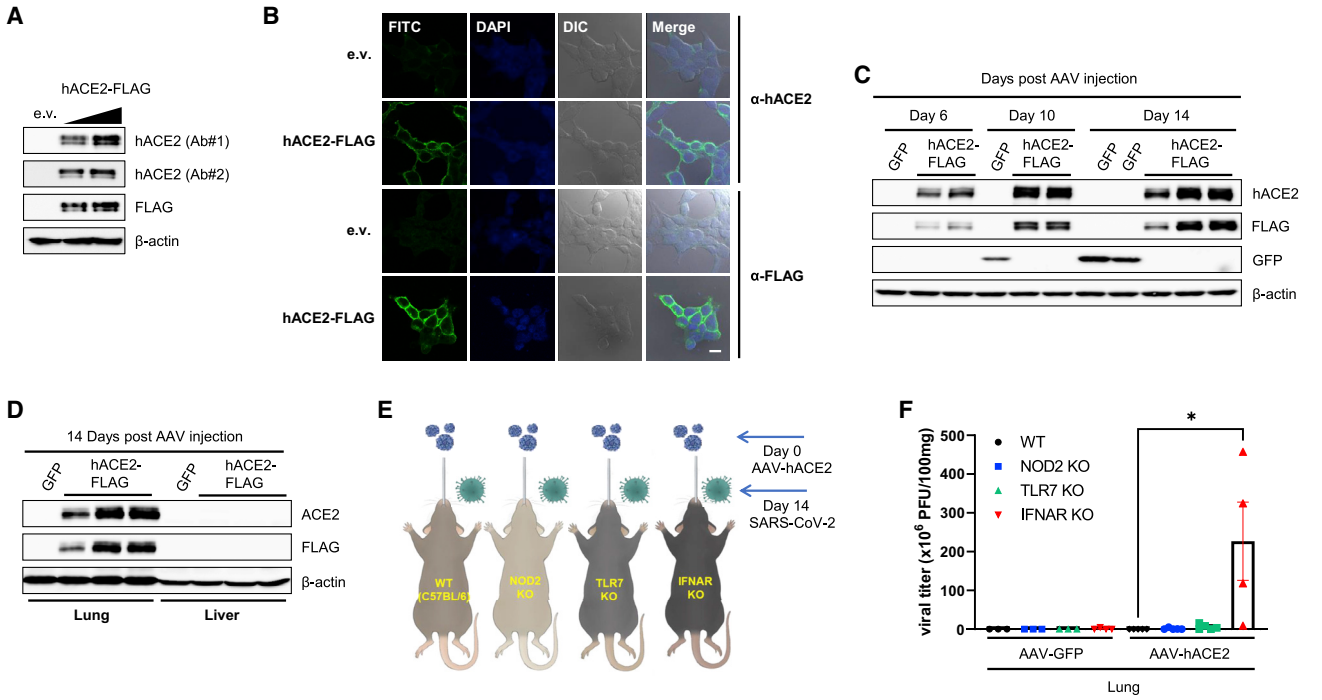

Figure 2. Mice with lungs expressing hACE2 are susceptible to SARS-CoV-2

(A and B) pcDNA3-hACE2-FLAG or empty vectors (e.v.) were transfected into HEK293T cells, and expression was analyzed 24 h post-transfection. (A) Western blotting analysis using 2 kinds of hACE2 antibodies and FLAG or β-actin antibodies. (B) Confocal microscopy images of the transfected cells. hACE2 or FLAG (FITC, green), DAPI for nuclear staining (blue), differential interference contrast (DIC) images, and merged images are shown. Scale bar, 10 μm. (C and D) Mice were injected with AAV2/8-GFP or AAV2/8-hACE2, and the protein levels in the mice tissues were analyzed at 6, 10, and 14 days post-virus injection, as indicated. (E and F) Wild-type (WT), NOD2 knockout (KO), TLR7 KO, and IFNAR KO mice were administered AAV-GFP or AAV-hACE2 both intratracheally and intranasally. At 14 days post-AAV injection, the mice were injected with SARS-CoV-2 intranasally. (E) Schematic for administration viral injections into mice with timeline. (F) SARS-CoV-2 viral titer in the lungs of the mice. Values are presented as means ± standard errors of the mean.

Therefore, we decided to use 25 μL of 4×10^{11} VPs of AAV in subsequent experiments. Compared to intratracheal delivery, intranasal delivery via the upper respiratory tract could lead to an infection in the upper part of the respiratory system. Intranasal administration led to GFP expression in the nose (Figure S1D), indicating that intranasal injection could infect the whole respiratory tract. This suggests that intratracheal delivery of AAV aids in specifically targeting lung parenchyma and is a promising method for achieving the pulmonary expression of desired proteins. Next, we analyzed the efficiency of non-invasive intratracheal delivery compared to that of the invasive intratracheal method, which is a widely used delivery method for the lungs. GFP expression in the lungs of non-invasively administered mice was comparable to that of invasively administered mice (Figure S1E). In addition, to determine whether non-invasive intratracheal delivery of AAV would work in other rodents, Syrian hamsters were intratracheally injected with either AAV2/8-GFP or AAV2/9-GFP. Similar to mice, GFP expression was observed in the lungs, but not in the livers, of the hamsters injected with AAV (Figure S1F).

Besides tissue tropism, AAV vectors also show cell-type tropism. The lung tissue comprises various cells, including two types of parenchymal cells, namely AT1 and AT2. Thus, we looked into the cellular distribution of GFP after the intratracheal administration of AAV. Using confocal microscopy, GFP expression was found in the alveolar squamous cells (AT1) stained with Aquaporin5 (AQP5) and was found to colocalize with AT2 cells stained with prosurfactant protein-C (proSPC; Figure 1C); GFP expression was not merged with the vascular endothelial cells stained with von Willebrand factor (VWF). These results indicate that the intratracheal delivery of AAV2/8 targets both AT1 and AT2 cells but not vascular endothelial cells. We further analyzed the AAV2/9 cell-type tropism in the lung tissue (Figure S2A). Like AAV2/8, AAV2/9 showed similar cell-type tropism. The efficiency for targeting AT2 cells was found to be similar between the two serotypes (Figure S2B).

Susceptibility of AAV-hACE2 transduced mice to SARS-CoV-2 is enhanced by the deficiency of type I interferon (IFN) signaling

Based on the finding that intratracheal injection of AAV2/8 vector specifically targets lung parenchyma, we attempted to use it to develop SARS-CoV-2-susceptible mice. For this, hACE2 with a FLAG tag at the carboxy terminal was cloned, and its expression and membrane localization were confirmed in transfected 293T cells (Figures 2A and 2B). The open reading frame of the construct was then subcloned to generate the AAV2/8-expressing hACE2-FLAG

(AAV-hACE2). AAV-hACE2 or AAV-GFP, which was used as a control, was administered both intratracheally and intranasally, as the upper respiratory tract is a major route of transmission for SARS-CoV-2 infection.[15] After 2 weeks from administration, hACE2 expression was detected in the lung, but not in the liver, of mice, raising the possibility that this could be a useful model that can be quickly generated for SARS-CoV-2 (Figures 2C and 2D).

To investigate the factors that can affect SARS-CoV-2 infection, we used three kinds of immune function-relevant gene KO mice, which were namely KOs for the nucleotide-binding oligomerization domain 2 (NOD2), Toll-like receptor 7 (TLR7) and type I IFN receptor (IFNAR). Mice were transduced with hACE2 or GFP using AAV (AAV-hACE2/NOD2 KO, AAV-hACE2/TLR7 KO, and AAV-hACE2/IFNAR KO mice), followed by intranasal administration of SARS-CoV-2 2 weeks post-AAV infection (Figure 2E). When mice were transduced with AAV-hACE2, the SARS-CoV-2 titer in the lungs of AAV-hACE2/IFNAR KO mice was robustly and significantly increased compared to that in the AAV-hACE2 wild-type (WT) mice, while the viral titers in the AAV-hACE2/NOD2 KO and AAV-hACE2/TLR7 KO mice were comparable to those in the AAV-hACE2/WT mice (Figure 2F). The expression levels of hACE2 protein among the groups were similar (Figure S3A). SARS-CoV-2 was not detected in the lungs of GFP-transduced mice regardless of genotype, indicating that hACE2 is a genuine receptor for SARS-CoV-2 (Figure 2F). These results suggest the relevance of type I IFN signaling in protecting SARS-CoV-2 infection.

As AAV-hACE2/IFNAR KO mice were susceptible to SARS-CoV-2, we further analyzed the effect of AAV serotypes and invasiveness of intratracheal injections on viral replication. The viral titer was not influenced by AAV2/8 and AAV2/9 serotypes (Figure S3B). This result was supported by those obtained by confocal microscopy that both serotypes target AT2 cells with similar efficiency (Figure S2B). The administration method (non-invasive versus invasive) also did not alter the viral titer significantly (Figure S3B).

We also investigated how long hACE2 could be maintained in the lungs of AAV-hACE2-injected mice. Considering that the lifespan of AT1 cells and AT2 cells are 120 days and 28–35 days, respectively,[16,17] hACE2 signals are supposed to disappear gradually. However, hACE2 expression was maintained until 6 and 8 weeks after AAV injection, as determined by immunofluorescence and western blotting assays (Figures S4A and S4B). One reason for this could be the differentiation of AT2 cells expressing hACE2 to AT1 cells, which live longer and still express hACE2.[9]

SARS-CoV-2 protein is detected in tracheas and lungs of AAV-hACE2/IFNAR KO mice

To further analyze the relevance of type I IFN signaling in SARS-CoV-2 infection, we randomly divided IFNAR KO mice into four groups: AAV-GFP/IFNAR KO mice treated with Dulbecco's Modified Eagle Medium (DMEM) (GFP + media), AAV-hACE2/IFNAR KO mice treated with DMEM (hACE2 + media), AAV-GFP/IFNAR KO mice treated with SARS-CoV-2 (GFP + CoV-2), and AAV-hACE2/IFNAR KO mice treated with SARS-CoV-2 (hACE2 + CoV-2) (Figure 3A). These mice were sacrificed at 2, 4, or 7 days post-infection (DPI) of SARS-CoV-2. Body weight and temperature were not altered either by hACE2 transduction or SARS-CoV-2 infection (Figure S5). Nucleocapsid protein (NP) expression of SARS-CoV-2 was observed only in the tracheas and the lungs of the hACE2 + CoV2 group at 2 DPI (Figures 3B–3E). NP expression was not detected at 4 and 7 DPI, suggesting the clearance of SARS-CoV-2 by this time point (Figures 3B–3E).

SARS-CoV-2 causes multiple lesions in tracheas and lungs of AAV-hACE2/IFNAR KO mice

Histopathologic scoring of abnormalities and lesions in the trachea and lungs of the four groups of mice was compared. Pulmonary histology of the GFP + media, hACE2 + media, and GFP + CoV2 groups were normal at the different DPI (Figure 4A). However, in the hACE2 + CoV2 group, mild lesions were observed in the trachea at both 2 and 4 DPI, the tracheal epithelium was exfoliated, and the ciliated pseudostratified columnar epithelium was collapsed at 7 DPI (Figure 4A). Moreover, only the hACE2 + CoV2 group showed pulmonary lesions. Alveolar walls were thickened and mononuclear inflammatory cells were infiltrated around the peribronchiolar and perivascular regions at 2 and 4 DPI (Figures 4B–4D). At 7 DPI, it was observed that interstitial pneumonia was moderately infiltrated with immune cells around the perivascular regions, but that around the peribronchiolar regions was more severe (Figures 4B–4D). The infiltrated immune cells mostly comprised lymphocyte antigen 6 complex locus $G6D^{+}$ ($Ly6G^{+}$) monocytes and neutrophils with a minor population of $F4/80^{+}$ macrophages (Figure S6A–S6D). The histopathologic score of the hACE2 + CoV2 group was higher than that in the other three groups (Figures 4E–4F). These results indicate that AAV-hACE2/IFNAR mice are highly susceptible to SARS-CoV-2 infection (Figures 4E and 4F).

DISCUSSION

Several efforts have been made to target AAV-mediated gene delivery to the lung parenchyma. Tail-vein injection of AAV2-ESGHGYF, which is of serotype 2 with a modified ESGHGYF peptide in the capsid protein, has been shown to specifically target lung tissue.[18] However, the infected cells mainly merged with CD31-expressing cells, which are supposed to be vascular endothelial cells. Although Wang et al. and Kang et al. have reported that AAV8 and AAV6.2FF, which is of serotype 6 with 3-point mutations in the capsid protein, target the lung parenchyma, AAV administration was performed after tracheotomy.[19,20] Santry et al. reported that the intubation method effectively targets lung tissue.[21] Non-invasive intratracheal administration used in the present study is expected to be similarly efficient when compared to the intubation method, but takes <1 min to inject per mouse and can be conducted under mild anesthesia without any invasive surgery. This implies that simply altering the administration method could be efficient enough to target lung parenchyma. The method we used here also targeted the lungs of hamsters, suggesting its potential application in a diverse range of experimental animals.

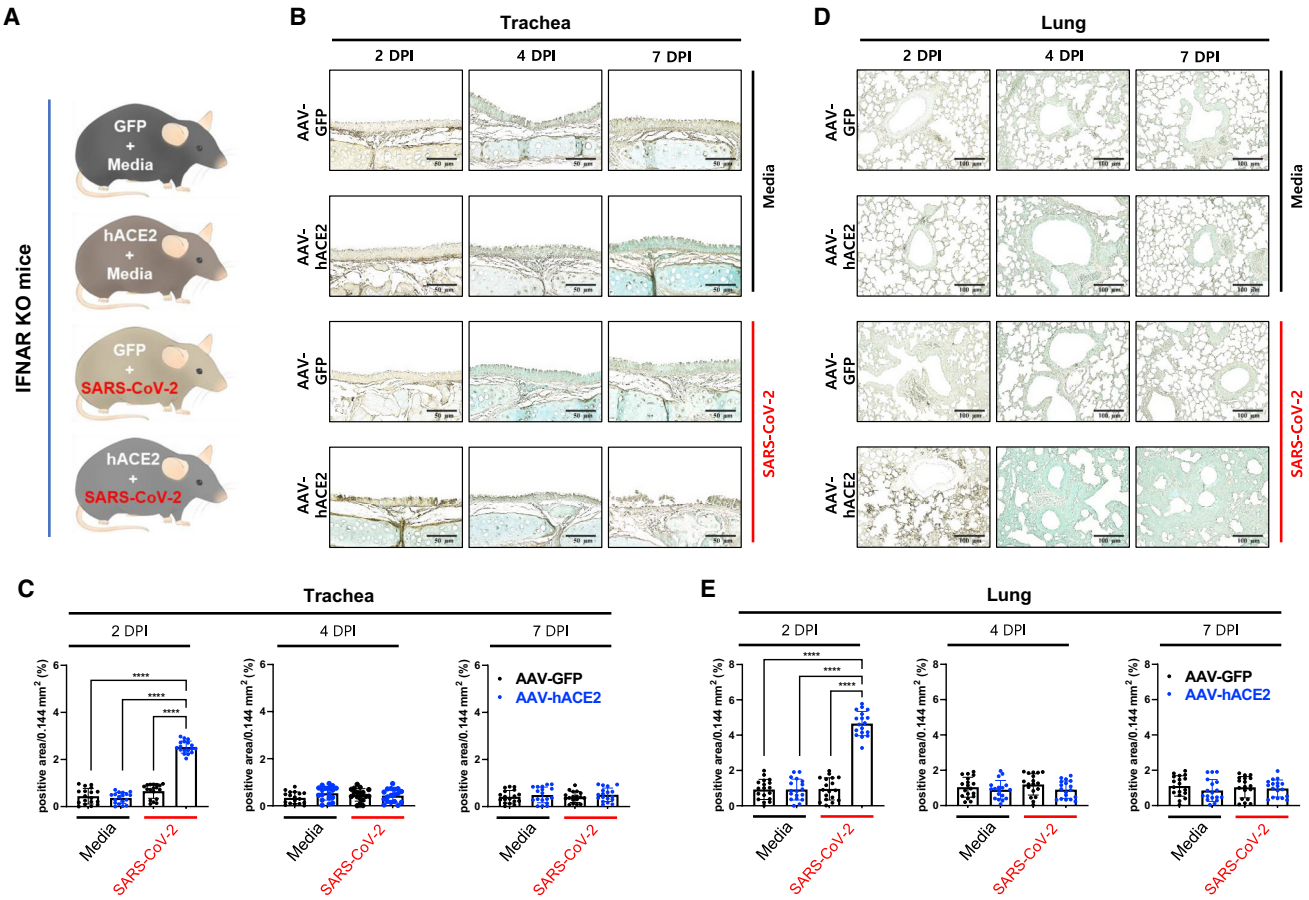

Figure 3. SARS-CoV-2 nucleocapsid protein is detected in tracheas and lungs of AAV-hACE2/SARS-CoV-2 IFNAR KO mice

(A) IFNAR KO mice were divided into 4 groups as follows: AAV-GFP + media, AAV-GFP + SARS-CoV-2, AAV-hACE2 + media, and AAV-hACE2 + SARS-CoV-2. (B and D) Immunohistochemistry of tracheal and lung tissue of the mice using antibodies against nucleocapsid protein of SARS-CoV-2 at 2, 4, and 7 days post-infection. Scale bars, 50 μm (B) and 100 μm (D). (C and E) Percentages of stained area were scored. All of the values are presented as means ± standard deviations. ****$p < 0.0001$.

Intranasal injection of AAV induced levels of GFP expression in the lung similar to that seen with intratracheal injection. However, intranasal administration also led to the infection of the upper respiratory tract (Figure S1D). Therefore, although intratracheal injection more specifically targets the lung parenchyma, intranasal injection would be presumably more useful in generating some other animal models. For instance, intranasal administration could be more effective in studying a protein that has protective functions against infectious diseases in either the upper respiratory tract and/or whole respiratory system, probably with minor adjustments in viral concentrations and/or volume. In addition, as in the present study, intranasal administration of AAV vector would be useful to express viral receptors in the upper respiratory tract.

The lungs are composed of multiple lobes. For western blotting, we used the right-inferior lobe, which is most distal from the trachea. The strong expression of GFP in the inferior lobe indicates that a single injection of 4×10^{11} VPs of AAV in a 25-μL volume is enough to infect all parts of the lung. Injection of a higher dose (2×10^{12} VPs of AAV) in a higher volume (50 μL) led to a higher expression of GFP in the liver (Figure S1C), probably because the high concentration of VP and high instillation volume results in the penetration of the alveolar-capillary barrier by AAV, followed by circulation in the bloodstream. Based on our results, 4×10^{11} VPs of AAV in a 25-μL volume is suitable for targeting the expression of GFP in the lungs of 8-week-old male C57BL/6 mice. The instillator with a micro-camera, used in this study, was initially developed for pulmonary delivery of irritants such as fine dust. We also found it very useful to deliver a small volume of virus inside a trachea, and the efficacy of target protein expression using this system was comparable to that using an invasive method (Figure S3B). We, however, believe using a machine is not essential to deliver the virus, since a few publications have reported using a manual method without an automatic instillator, suggesting that intratracheal injection is a non-invasive and easy method that can be used widely.[22–24]

Intratracheal injection could be widely adopted in various fields of research. In the present study, we revealed that this system can be

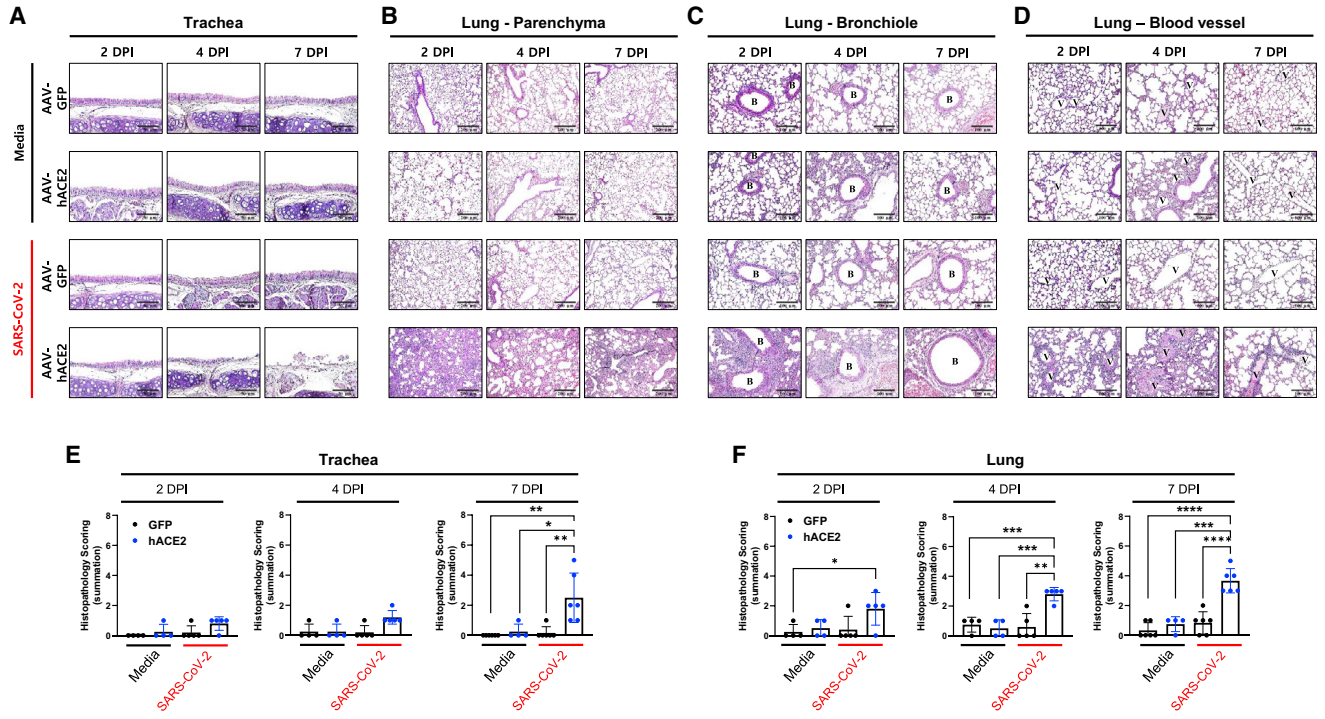

Figure 4. SARS-CoV-2 causes multiple lesions in the trachea and lungs of AAV-hACE2/SARS-CoV-2 IFNAR KO mice

(A–D) Histopathology of IFNAR KO mice expressing GFP or hACE2 in the respiratory system after injection of either SARS-CoV-2 or media. Images of tracheal and lung tissue (parenchyma, bronchiole, and blood vessel) of the mice at 2, 4, and 7 days post-infection. B, bronchiole; V, vessel. Scale bars, 50 μm (A), 200 μm (B), and 100 μm (C and D). (E and F) The extent of lesions and severity was quantified and summation of the histopathology scores was completed. All of the values are presented as means ± standard deviations. *p < 0.05, **p < 0.01, ***p < 0.001, ****p < 0.0001.

used to generate animal models susceptible to infectious disease. Previous studies reported that adenovirus-mediated hACE2-transduced mice are susceptible to SARS-CoV-2 infection.[25,26] However, unlike the AAV vector, the administration of adenoviral vector causes severe innate inflammatory responses and may be toxic.[27] Recently, Israelow et al. showed that AAV serotype 9-mediated hACE2-transduced WT and IFNAR KO mice are more susceptible to SARS-CoV-2, and this finding is similar to our study, although with a different administration method.[28] In their study, AAV was invasively injected into the trachea during surgery, implying that the procedure may hinder the recovery of mice, especially IFNAR KO mice, which are also immunocompromised. Interestingly, Israelow et al. observed the viral titer in the lungs of IFNAR KO mice was comparable to that of WT mice.[28] In contrast, our study showed a robust increase in SARS-CoV-2 viral titer with microscopic lesions in the lungs of IFNAR KO mice. The discrepancy may come from the differences in administration procedures (non-invasive versus invasive), hACE2 expression amount (AAV2/8 versus AAV9), and/or SARS-CoV-2 strain (NCCP-43331 versus NR-52281). However, in the present study, we found that non-invasive and invasive delivery of AAV-hACE2 caused similar levels of SARS-CoV-2 replication, and serotypes AAV2/8 and AAV2/9 did not influence the viral titer (Figure S3B). Given the importance of type I IFN response against SARS-CoV-2 infection,[29–31] increased SARS-CoV-2 virus in the background of IFNAR deficiency is not surprising. In line with the increased viral titer and NP levels, we observed significant lesions in the trachea and lung in the AAV-hACE2/IFNAR KO mice infected with SARS-CoV-2 virus in the present study. We expect that IFNAR KO mice transduced with AAV2/8-hACE2 could be a useful model for future SARS-CoV-2 research.

We also investigated the relevance of TLR7 and NOD2 in SARS-CoV-2 pathogenesis. Since SARS-CoV-2 is a single-stranded RNA, we predicted that it may be recognized by TLR7 effectively.[32,33] The role of NOD2 in the activation of innate immune antiviral response is well characterized.[34] Moreover, TLR7 and NOD2 are potently relevant to type I IFN signaling.[35,36] However, SARS-CoV-2 viral titer was found to increase only in the IFNAR KO mice and not in the TLR7 KO or NOD2 KO mice. These results may suggest that TLR7 and NOD2 are not implicated in the replication of SARS-CoV-2, and further studies would be needed.

Interestingly, despite the lack of NP in the trachea and lung at 4 and 7 DPI, the most marked lesions were observed at 7 DPI (Figures 3 and 4). We speculate that the increase in cytokine release induced by the hyperactivation of infiltrated inflammatory cells is the main cause of the lesions.[37] Interestingly, the pathological symptoms of SARS-CoV-2 infection in AAV2/8-hACE2 mice were not so severe

as those in K18-hACE2 or HFH4-hACE2 transgenic mice,[38,39] probably because of the neuroinvasion of SARS-CoV-2 in the aforementioned transgenic mice.[39,40] We should mention that AAV2/8-hACE2 mice express hACE2 mainly in the lung tissue (Figure 1D).

In the present study, we revealed that intratracheally administered AAV infects lung parenchymal cells, including AT2, which is highly susceptible to SARS-CoV-2.[41] Given the vector we used, GFP expression is controlled by the *CAG* promoter, which is a ubiquitously active promoter for constitutive expression. If we replace the *CAG* promoter with an *Aqp5* promoter or *Sftpc* promoter,[42,43] which is specifically activated in AT1 or AT2, respectively, the more specific cell-type expression could be achieved by intratracheal delivery of AAV2/8. Given that SARS-CoV-2 primarily infects AT2 cells highly expressing ACE2,[44] mice transducing hACE2 under the *Sftpc* promoter would be a more suitable model for SARS-CoV-2 studies. Future studies would be required to address the promoter-dependent specific expression in AT1 and AT2 cells. In this study, we reveal that the system is suitable for inducing protein overexpression in the pulmonary parenchyma. However, this system can be also adapted for knockdown or knockout of gene expression. If AAV containing small hairpin RNA under *U6* or *H1* promoter, instead of GFP under *CAG* promoter, was used, it could knock down the expression of the endogenous mRNA of the target gene. Otherwise, guide RNA containing AAV could be intratracheally injected into CRISPR-associated protein 9 transgenic mice to achieve specific gene deletion in the lung parenchymal cells.

In conclusion, we found that intratracheal administration of AAV2/8 targets pulmonary parenchymal cells, including AT2 cells. This approach specifically targets the lung tissue. We used this system for the delivery of hACE2 to the lung tissue of various immune function-relevant gene KO mice. Following SARS-CoV-2 infection to these mice, we identified type I IFN signaling, but not NOD2 and TLR7, to have a protective effect against SARS-CoV-2 pathogenesis. Since this method is easy and quick to apply, we speculate that it will be widely used to study diverse pulmonary diseases.

MATERIALS AND METHODS

Biosafety

Except for AAV vector transduction, all of the animal experiments, including maintenance of the animal colony, infection, physical examination, and necropsy, were performed in an animal biosafety level III (ABSL3) facility of the Korea Zoonosis Research Institute (KOZRI) at Jeonbuk National University. Researchers involved in this study were approved and qualified for ABSL3 experiments by KOZRI and/or the Bioethics Information Center. All of the experimental procedures were reviewed and approved by the animal ethics committee of Jeonbuk National University (CBNU 2020-056).

Preparation of infectious SARS-CoV-2 virus

SARS-CoV-2 (NCCP-43331) was provided by the National Culture Collection for Pathogens, Korea. The virus was cultured in Vero E6 cells and all of the experimental procedures associated with virus handling were conducted in a BSL3 facility, KOZRI, Jeonbuk National University. Viral stocks were prepared by propagating in Vero E6 cells cultured in DMEM supplemented with 2% fetal bovine serum, 1% penicillin-streptomycin, and HEPES (Invitrogen). Viral titers were determined by estimating the median tissue culture infectious dose.

Transfection of hACE2 to 293T cells

293T cells were transfected with pcDNA3-hACE2-FLAG (or empty vector) construct using Lipofectamine 3000 (Thermo Fisher), according to the manufacturer's instructions.

Preparation and purification of AAVs

AAVs were generated by co-transfection of pAAV vector containing either GFP or hACE2 gene, pAAV2/8 (#112864) or pAAV2/9 (#112865), and helper plasmid pAdDeltaF6 (#112867; Addgene) in a 1:1:1 molar ratio using polyetherimide. The cell culture media were changed 16 h later, and the cells were harvested at 72 h post-transfection. The harvested cells were lysed in AAV lysis buffer (150 mM NaCl, 20 mM Tris pH 8.0) through 3 cycles of freezing and thawing, followed by incubation with Benzonase (E8263, Sigma-Aldrich) for the removal of nucleic acid, and centrifugation. For purification, the supernatant containing viruses was transferred to the top of the iodixanol gradient (15%, 25%, 40%, and 60%) in a QuickSeal tube and centrifuged at 280,000 × *g* for 3 h at 14°C (Himac CP80WX, P90AT rotor, Hitachi). The viral fraction was collected by puncturing the QuickSeal tube at the interface of the 60% and 40% gradients with an 18G needle. The collected viruses were concentrated using Amicon Ultra-15 Centrifugal Filter Unit (UFC910096, Sigma-Aldrich) and washed 2 times with PBS containing 0.1% Poloxamer 188 (P5556, Sigma-Aldrich) and 3 times with PBS. For AAV titration, 5 μL of the virus were incubated with DNase and proteinase K sequentially to eliminate any plasmid DNA carried over. Then, the number of genome-containing particles of an AAV was determined by quantitative PCR (CFX96, Bio-Rad).

Animal experiments

In this study, we used 6- to 8-week-old WT, TLR7KO, and IFNAR KO male mice.[36] NOD2 KO mice were kindly provided by Professor Jong-Hwan Park (College of Veterinary Medicine, Chonnam National University, Gwangju, Korea). Six-week-old Syrian hamsters were obtained from Central Lab Animal (Seoul, South Korea). All of the animals were kept in specific pathogen-free conditions and ventilated cages. The cages were maintained under a 12:12 light:dark cycle at 24 ± 2°C with 50% ± 5% humidity. All of the mice were kept in an ABSL3 facility for at least 2 days for stabilization and adaptation.

Six to 10 AAV-hACE2-transduced and SARS-CoV-2-infected WT, TLR7 KO, NOD2 KO, or IFNAR KO mice were group housed. Mice of each genetic background were divided into two subgroups: hACE2 transduced and control mice.

IFNAR KO mice were divided into four subgroups based on the transduction of hACE2 and infection of SARS-CoV-2: (1)

AAV-GFP/IFNAR KO mice injected with DMEM (GFP + media); (2) AAV-hACE2/IFNAR KO mice injected with DMEM (hACE2 + media); (3) AAV-GFP/IFNAR KO mice injected with SARS-CoV-2 (GFP + CoV-2); and (4) AAV-hACE2/IFNAR KO mice injected with SARS-CoV-2 (hACE2 + CoV-2). Mice transduced with AAV-GFP and injected with DMEM were used as controls. Body temperature and body weight were measured daily from the first day of infection to 7 DPI. Tracheal and lung tissues were harvested for analysis. At 2, 4, and 7 DPI, mice were sacrificed. Exsanguination was performed by cutting a caudal vena cava, followed by the careful isolation of tracheal and lung tissue.

AAV-hACE2 transduction

Non-invasive injection

Mice were lightly anesthetized using an isoflurane vaporizer chamber. In ventrodorsal recumbency, AAV-hACE2 or control (AAV-GFP) mice were injected intratracheally with $\sim 4 \times 10^{11}$ VPs per mouse under a micro-camera. After 6 h, mice were intranasally inoculated with 4×10^{11} VP of AAV-hACE2 or AAV-GFP using a pipette.

To perform invasive injection (tracheotomy and intratracheal instillation of AAV-hACE2), Zoletil (25 mg/kg; mixture of zolazepam and tiletamine, Zoletil 50, Virbac) was administered via intramuscular injection for anesthesia. After shaving the throat region with a razor blade, the site was scrubbed with 10% povidone-iodine solution. Pinnal-pedal reflex was used to assess the depth of anesthesia. The head and four limbs were fixed with plaster strips. To expose the cervical trachea, a 1.5-cm-long ventral cervical midline incision was made from the larynx to the sternum. Thyroid gland, sternohyoid muscles, and peritracheal tissues were bluntly separated and pulled aside carefully to avoid traumatizing the nerves, vessels, and esophagus. After full exposure of the ventral side of the trachea, 4×10^{11} VPs of AAV-hACE2 or AAV-GFP were injected using an insulin syringe (31G needle). After infection, the skin incision line was washed with sterile saline and closed using a surgeon's knot with 6/0 non-absorbable suture. To protect the wound and prevent contamination, the throat region was scrubbed with 10% povidone-iodine solution and then a liquid bandage was applied. After 6 h, mice were intranasally inoculated with 4×10^{11} VPs of AAV-hACE2 or AAV-GFP using a pipette.

Intranasal inoculation with SARS-CoV-2

One week after AAV vector transduction, mice under light isoflurane anesthesia were intranasally inoculated with 1×10^6 plaque-forming units (PFUs) of SARS-CoV-2 in 30 μL DMEM using a pipette in an ABSL3 facility.

Protein extraction and immunoblotting

Tissues were homogenized and cells were lysed using radioimmunoprecipitation buffer (150 mM NaCl, 50 mM Tris, pH 8.0, 0.5% sodium deoxycholate, 0.1% sodium dodecyl sulfate, and 1X NP-40) containing protease inhibitor cocktail (11836153001, Sigma-Aldrich). Protein levels were quantified using DC Protein Assay Reagents (5000116, Bio-Rad). Lysates were subjected to sodium dodecyl sulfate-polyacrylamide gel electrophoresis and transferred onto nitrocellulose membranes. The blots were incubated with antibodies against either ACE2 (A4612, monoclonal, and A12737, polyclonal, ABclonal), FLAG (PA1-984B, Thermo Fisher), or GFP (ab290, Abcam) and processed using standard protocols. β-Actin (sc-47778, Santa Cruz Biotechnology) and HSP90 (#4874, Cell Signaling Technology) were used as the loading control.

Immunofluorescence

293T cells cultured on cover slides were transfected with empty vector or hACE2-FLAG and then fixed with 10% neutral-buffered formalin (HT501128, Sigma-Aldrich). After 3 washes with PBS, the cells were permeabilized with 0.1% Triton X-100 and incubated with FLAG antibody (1:300, PA1-984B, Thermo Fisher) overnight on a rocker at 4°C. For ACE2 (A12737, Abclonal) immunofluorescence, the permeabilization step was skipped. After primary incubation, the cells were probed with a fluorescein isothiocyanate (FITC)-conjugated secondary antibody (A16995, Thermo Fisher). Washed samples were mounted with ProLong Gold containing DAPI (P36941, Thermo Fisher), and images were acquired using a confocal microscope (LSM 900, Carl Zeiss, Oberkochen, Germany).

Determination of the viral titer

Plaque assay was performed to determine the infectious titer of SARS-CoV-2. Vero E6 cells were seeded in a 12-well plate at 2×10^5 cells/well and cultured overnight in a CO_2 incubator. The supernatant of homogenized tissues was serially 10-fold diluted (from 10^1 to 10^6) and applied to the culture plate. After 1 h of incubation, the supernatant was removed. Each well was washed with PBS and 1.5 mL of media was overlaid. The culture plate was incubated for another 3 days in a CO_2 incubator. Cells were then fixed with 1 mL 4% formalin and stained with 0.4% Crystal Violet in 70% methanol in PBS. Viral titer was calculated by counting the number of plaques.

Histopathology and immunohistochemistry

Formalin-fixed samples were routinely processed and embedded in paraffin wax (Surgipath Paraplast, Leica Biosystems). Formalin-fixed paraffin-embedded tissue blocks were sectioned at 4-μm-thick sections using a standard rotary microtome (HM-340E, Thermo Fisher). Tissue sections were stained with hematoxylin and eosin.

Abnormalities in the tracheal and pulmonary tissue were scored using representative microscopic lesions. Scoring criteria ranged from 0 to 3 based on the severity or proportion of the lesioned tissue: 0, none-to-rare or <10%; 1, mild or 10%–40%; 2, moderate or 40%–70%; and 3, severe or >70%. Tracheal abnormalities were scored using the following criteria: (1) inflammation of lamina propria; (2) cellular exudates in tracheal lumen; and (3) tracheal epithelium damage. Lung abnormalities were scored using the following criteria: (1) inflammation of the peribronchiolar region; (2) inflammation of the perivascular region; (3) cellular exudates in bronchiolar lumen; (4) bronchiolar epithelium damage; (5) thickening of the alveolar wall (interstitial pneumonia); and (6) hemorrhage. While scoring, care was taken

because lesions were not evenly distributed across the entire tissue and showed various patterns. The final score was the sum of scores under each criterion; a high score indicated a higher degree of microscopic damage. The criteria used for scoring are categorized and summarized in Table S1.

For immunohistochemistry, a silane-coated slide was used for its strong adhesiveness. To re-establish immunoactivity, antigen retrieval was conducted using citrate buffer (pH 6.0) at 95°C for 30 min and at room temperature for 20 min. Sections were then incubated overnight at 4°C with a SARS-CoV-2 NP antibody (40,143-V08B, Sino Biological) or Ly6G (14-5931-82, Thermo Fisher), and F4/80 (SC-25830, Santa Cruz Biotechnology) diluted to 1:500 using an antibody diluent (E09-300, GBI Labs). To label SARS-CoV-2 NP, Ly6G, and F4/80, horseradish peroxidase-conjugated anti-rabbit and anti-rat immunoglobulin G (IgG) antibodies (MP-7500 and MP-7404, Vector Laboratories) were used. The antibody was visualized with 3,3′-diaminobenzidine (SK-4105, Vector Laboratories) at the concentration recommended by the manufacturers. Tissues were counterstained with methyl green. All of the slides were examined (BX53, Olympus) and imaged (DP80, Olympus) microscopically using a light microscope. All histopathologic examinations were conducted in a double-blind fashion with trained pathologists. To quantify immunohistochemical results, image analysis was performed using TS Auto 5.1 (Olympus). The percentage of immunopositive area was analyzed at a defined magnification and area (400 magnification field, 0.144 mm^2).

For immunofluorescence staining, we used the method of intratracheal instillation of the fixative. Briefly, tracheostomy was performed, and an 18G needle tip was inserted into the trachea. Lungs were inflated via cannula by gentle infusion of 10% neutral buffered formalin at a constant fluid pressure of 25 cm for 20 min. After tying off the trachea, the lungs were kept in a 50-mL tube containing 10% neutral buffered formalin (NBF) for 6 h, and then, transferred to a new tube containing pre-chilled cryoprotection solution (20% sucrose and 33% OCT [optimal cutting temperature] compound) and kept overnight. The following day, the lungs were embedded in OCT compound and snap-frozen. Cryosections (8-μm-thick) were prepared using a cryostat. For staining, cryosections were blocked with 5% normal donkey serum in PBS containing 0.3% Triton X-100 (PBS-T) and incubated overnight at 4°C with the following antibodies in PBS-T: rabbit anti-AQP5 (#ab78486, Abcam), rabbit anti-proSPC (#AB3786, Sigma-Aldrich), rabbit anti-VWF (#PA5-16634, Thermo Fisher), rabbit anti-ACE2 (#A12737, ABclonal), chicken anti-GFP (#ab13970, Abcam). The next day, the sections were washed with PBS for 2 h and incubated for 90 min with the following secondary antibodies in PBS containing 0.1% Triton X-100 and 0.1% Tween 20: donkey anti-rabbit (#A31573, Thermo Fisher) or donkey anti-chicken (#703-545-155, Jackson ImmunoResearch). After washes with PBS for 90 min, samples were mounted with ProLong Gold containing DAPI (P36941, Thermo Fisher), and images were acquired using a confocal microscope (LSM 900, Carl Zeiss).

Statistical analysis

All of the data are expressed as means ± standard deviations. One-way analysis of variance was used to test for statistical significance among experiment groups followed by Duncan's multiple range test for multiple comparisons as a post hoc test. Asterisks indicate significant differences among the groups ($^{*}P \leq 0.05$, $^{**}P \leq 0.01$, $^{***}P \leq 0.001$, and $^{****}P \leq 0.0001$). All of the statistical analyses were carried out using SAS version 9.4 (SAS Institute, Cary, NC, USA). The data were plotted using GraphPad Prism version 9.1.1 (GraphPad Software).

SUPPLEMENTAL INFORMATION

Supplemental information can be found online at https://doi.org/10.1016/j.ymthe.2022.01.010.

ACKNOWLEDGMENTS

This research was supported by the Basic Science Research Program through the National Research Foundation of Korea (NRF) funded by the Ministry of Education (NRF-2019R1A6A1A03033084, to B. K.), the Ministry of Science and ICT (NRF-2019R1C1C1007040, to D.-i. K.), NRF-2020R1A4A1019395 (to M.-J. P.), and the research program funded by the Korea Disease Control and Prevention Agency (fund code no. 2020-ER5321-00, to K.-S. L.).

AUTHOR CONTRIBUTIONS

M.-S.Y., M.-J.P., J.L., D.-i.K., and B.K. designed the experiments. M.-S.Y., M.-J.P., J.L., B.O., K.W.K., Y.K., S.-M.L., J.-O.L., T.-Y.J., J.-H.P., S.-C.P., Y.-S.L., S.B.H., and K.-S.L. performed the experiments and analyzed the data. M.-S.Y., M.-J.P., J.L., D.-i.K., and B.K. wrote the manuscript. D.-i.K. and B.K. supervised the project.

DECLARATION OF INTERESTS

The authors declare no competing interests.

REFERENCES

1. Wang, D., Tai, P.W.L., and Gao, G. (2019). Adeno-associated virus vector as a platform for gene therapy delivery. Nat. Rev. Drug Discov. *18*, 358–378. https://doi.org/10.1038/s41573-019-0012-9.

2. Li, C., and Samulski, R.J. (2020). Engineering adeno-associated virus vectors for gene therapy. Nat. Rev. Genet. *21*, 255–272. https://doi.org/10.1038/s41576-019-0205-4.

3. Zincarelli, C., Soltys, S., Rengo, G., and Rabinowitz, J.E. (2008). Analysis of AAV serotypes 1-9 mediated gene expression and tropism in mice after systemic injection. Mol. Ther. *16*, 1073–1080. https://doi.org/10.1038/mt.2008.76.

4. Gao, G.P., Alvira, M.R., Wang, L., Calcedo, R., Johnston, J., and Wilson, J.M. (2002). Novel adeno-associated viruses from rhesus monkeys as vectors for human gene therapy. Proc. Natl. Acad. Sci. U S A *99*, 11854–11859. https://doi.org/10.1073/pnas.182412299.

5. Nathwani, A.C., Tuddenham, E.G., Rangarajan, S., Rosales, C., McIntosh, J., Linch, D.C., Chowdary, P., Riddell, A., Pie, A.J., Harrington, C., et al. (2011). Adenovirus-associated virus vector-mediated gene transfer in hemophilia B. N. Engl. J. Med. *365*, 2357–2365. https://doi.org/10.1056/NEJMoa1108046.

6. Rock, J.R., and Hogan, B.L. (2011). Epithelial progenitor cells in lung development, maintenance, repair, and disease. Annu. Rev. Cell Dev. Biol. *27*, 493–512. https://doi.org/10.1146/annurev-cellbio-100109-104040.

7. Yang, J., Hernandez, B.J., Martinez Alanis, D., Narvaez del Pilar, O., Vila-Ellis, L., Akiyama, H., Evans, S.E., Ostrin, E.J., and Chen, J. (2016). The development and

plasticity of alveolar type 1 cells. Development *143*, 54–65. https://doi.org/10.1242/dev.130005.

8. Fehrenbach, H. (2001). Alveolar epithelial type II cell: defender of the alveolus revisited. Respir. Res. *2*, 33–46. https://doi.org/10.1186/rr36.

9. Barkauskas, C.E., Cronce, M.J., Rackley, C.R., Bowie, E.J., Keene, D.R., Stripp, B.R., Randell, S.H., Noble, P.W., and Hogan, B.L. (2013). Type 2 alveolar cells are stem cells in adult lung. J. Clin. Invest. *123*, 3025–3036. https://doi.org/10.1172/jci68782.

10. Lu, R., Zhao, X., Li, J., Niu, P., Yang, B., Wu, H., Wang, W., Song, H., Huang, B., Zhu, N., et al. (2020). Genomic characterisation and epidemiology of 2019 novel coronavirus: implications for virus origins and receptor binding. Lancet *395*, 565–574. https://doi.org/10.1016/s0140-6736(20)30251-8.

11. Shang, J., Ye, G., Shi, K., Wan, Y., Luo, C., Aihara, H., Geng, Q., Auerbach, A., and Li, F. (2020). Structural basis of receptor recognition by SARS-CoV-2. Nature *581*, 221–224. https://doi.org/10.1038/s41586-020-2179-y.

12. Hoffmann, M., Kleine-Weber, H., Schroeder, S., Krüger, N., Herrler, T., Erichsen, S., Schiergens, T.S., Herrler, G., Wu, N.H., Nitsche, A., et al. (2020). SARS-CoV-2 cell entry depends on ACE2 and TMPRSS2 and is blocked by a clinically proven protease inhibitor. Cell *181*, 271–280.e8. https://doi.org/10.1016/j.cell.2020.02.052.

13. Letko, M., Marzi, A., and Munster, V. (2020). Functional assessment of cell entry and receptor usage for SARS-CoV-2 and other lineage B betacoronaviruses. Nat. Microbiol. *5*, 562–569. https://doi.org/10.1038/s41564-020-0688-y.

14. McCray, P.B., Jr., Pewe, L., Wohlford-Lenane, C., Hickey, M., Manzel, L., Shi, L., Netland, J., Jia, H.P., Halabi, C., Sigmund, C.D., et al. (2007). Lethal infection of K18-hACE2 mice infected with severe acute respiratory syndrome coronavirus. J. Virol. *81*, 813–821. https://doi.org/10.1128/jvi.02012-06.

15. Sungnak, W., Huang, N., Bécavin, C., Berg, M., Queen, R., Litvinukova, M., Talavera-López, C., Maatz, H., Reichart, D., Sampaziotis, F., et al. (2020). SARS-CoV-2 entry factors are highly expressed in nasal epithelial cells together with innate immune genes. Nat. Med. *26*, 681–687. https://doi.org/10.1038/s41591-020-0868-6.

16. Uhal, B.D. (1997). Cell cycle kinetics in the alveolar epithelium. Am. J. Physiol. *272*, L1031–L1045. https://doi.org/10.1152/ajplung.1997.272.6.L1031.

17. Williams, M.C. (2003). Alveolar type I cells: molecular phenotype and development. Annu. Rev. Physiol. *65*, 669–695. https://doi.org/10.1146/annurev.physiol.65.092101.142446.

18. Körbelin, J., Sieber, T., Michelfelder, S., Lunding, L., Spies, E., Hunger, A., Alawi, M., Rapti, K., Indenbirken, D., Müller, O.J., et al. (2016). Pulmonary targeting of adeno-associated viral vectors by next-generation sequencing-guided screening of random capsid displayed peptide libraries. Mol. Ther. *24*, 1050–1061. https://doi.org/10.1038/mt.2016.62.

19. Kang, M.H., van Lieshout, L.P., Xu, L., Domm, J.M., Vadivel, A., Renesme, L., Mühlfeld, C., Hurskainen, M., Mižíková, I., Pei, Y., et al. (2020). A lung tropic AAV vector improves survival in a mouse model of surfactant B deficiency. Nat. Commun. *11*, 3929. https://doi.org/10.1038/s41467-020-17577-8.

20. Liqun Wang, R., McLaughlin, T., Cossette, T., Tang, Q., Foust, K., Campbell-Thompson, M., Martino, A., Cruz, P., Loiler, S., Mueller, C., and Flotte, T.R. (2009). Recombinant AAV serotype and capsid mutant comparison for pulmonary gene transfer of alpha-1-antitrypsin using invasive and noninvasive delivery. Mol. Ther. *17*, 81–87. https://doi.org/10.1038/mt.2008.217.

21. Santry, L.A., Ingrao, J.C., Yu, D.L., de Jong, J.G., van Lieshout, L.P., Wood, G.A., and Wootton, S.K. (2017). AAV vector distribution in the mouse respiratory tract following four different methods of administration. BMC Biotechnol. *17*, 43. https://doi.org/10.1186/s12896-017-0365-2.

22. Driscoll, K.E., Costa, D.L., Hatch, G., Henderson, R., Oberdorster, G., Salem, H., and Schlesinger, R.B. (2000). Intratracheal instillation as an exposure technique for the evaluation of respiratory tract toxicity: uses and limitations. Toxicol. Sci. *55*, 24–35. https://doi.org/10.1093/toxsci/55.1.24.

23. Revelli, D.A., Boylan, J.A., and Gherardini, F.C. (2012). A non-invasive intratracheal inoculation method for the study of pulmonary melioidosis. Front. Cell Infect. Microbiol. *2*, 164. https://doi.org/10.3389/fcimb.2012.00164.

24. Ortiz-Muñoz, G., and Looney, M.R. (2015). Non-invasive intratracheal instillation in mice. Bio Protoc. *5*. https://doi.org/10.21769/bioprotoc.1504.

25. Hassan, A.O., Case, J.B., Winkler, E.S., Thackray, L.B., Kafai, N.M., Bailey, A.L., McCune, B.T., Fox, J.M., Chen, R.E., Alsoussi, W.B., et al. (2020). A SARS-CoV-2 infection model in mice demonstrates protection by neutralizing antibodies. Cell *182*, 744–753.e4. https://doi.org/10.1016/j.cell.2020.06.011.

26. Sun, J., Zhuang, Z., Zheng, J., Li, K., Wong, R.L., Liu, D., Huang, J., He, J., Zhu, A., Zhao, J., et al. (2020). Generation of a broadly useful model for COVID-19 pathogenesis, vaccination, and treatment. Cell *182*, 734–743.e5. https://doi.org/10.1016/j.cell.2020.06.010.

27. Ahi, Y.S., Bangari, D.S., and Mittal, S.K. (2011). Adenoviral vector immunity: its implications and circumvention strategies. Curr. Gene Ther. *11*, 307–320. https://doi.org/10.2174/156652311796150372.

28. Israelow, B., Song, E., Mao, T., Lu, P., Meir, A., Liu, F., Alfajaro, M.M., Wei, J., Dong, H., Homer, R.J., et al. (2020). Mouse model of SARS-CoV-2 reveals inflammatory role of type I interferon signaling. J. Exp. Med. *217*. https://doi.org/10.1084/jem.20201241.

29. Xia, H., Cao, Z., Xie, X., Zhang, X., Chen, J.Y., Wang, H., Menachery, V.D., Rajsbaum, R., and Shi, P.Y. (2020). Evasion of type I interferon by SARS-CoV-2. Cell Rep. *33*, 108234. https://doi.org/10.1016/j.celrep.2020.108234.

30. Lei, X., Dong, X., Ma, R., Wang, W., Xiao, X., Tian, Z., Wang, C., Wang, Y., Li, L., Ren, L., et al. (2020). Activation and evasion of type I interferon responses by SARS-CoV-2. Nat. Commun. *11*, 3810. https://doi.org/10.1038/s41467-020-17665-9.

31. Mantlo, E., Bukreyeva, N., Maruyama, J., Paessler, S., and Huang, C. (2020). Antiviral activities of type I interferons to SARS-CoV-2 infection. Antivir. Res. *179*, 104811. https://doi.org/10.1016/j.antiviral.2020.104811.

32. Lund, J.M., Alexopoulou, L., Sato, A., Karow, M., Adams, N.C., Gale, N.W., Iwasaki, A., and Flavell, R.A. (2004). Recognition of single-stranded RNA viruses by Toll-like receptor 7. Proc. Natl. Acad. Sci. U S A *101*, 5598–5603. https://doi.org/10.1073/pnas.0400937101.

33. Bauer, S., Pigisch, S., Hangel, D., Kaufmann, A., and Hamm, S. (2008). Recognition of nucleic acid and nucleic acid analogs by Toll-like receptors 7, 8 and 9. Immunobiology *213*, 315–328. https://doi.org/10.1016/j.imbio.2007.10.010.

34. Sabbah, A., Chang, T.H., Harnack, R., Frohlich, V., Tominaga, K., Dube, P.H., Xiang, Y., and Bose, S. (2009). Activation of innate immune antiviral responses by Nod2. Nat. Immunol. *10*, 1073–1080. https://doi.org/10.1038/ni.1782.

35. Pandey, A.K., Yang, Y., Jiang, Z., Fortune, S.M., Coulombe, F., Behr, M.A., Fitzgerald, K.A., Sassetti, C.M., and Kelliher, M.A. (2009). NOD2, RIP2 and IRF5 play a critical role in the type I interferon response to Mycobacterium tuberculosis. PLoS Pathog. *5*, e1000500. https://doi.org/10.1371/journal.ppat.1000500.

36. Roh, Y.S., Park, S., Kim, J.W., Lim, C.W., Seki, E., and Kim, B. (2014). Toll-like receptor 7-mediated type I interferon signaling prevents cholestasis- and hepatotoxin-induced liver fibrosis. Hepatology *60*, 237–249. https://doi.org/10.1002/hep.26981.

37. Fajgenbaum, D.C., and June, C.H. (2020). Cytokine storm. N. Engl. J. Med. *383*, 2255–2273. https://doi.org/10.1056/NEJMra2026131.

38. Bao, L., Deng, W., Huang, B., Gao, H., Liu, J., Ren, L., Wei, Q., Yu, P., Xu, Y., Qi, F., et al. (2020). The pathogenicity of SARS-CoV-2 in hACE2 transgenic mice. Nature *583*, 830–833. https://doi.org/10.1038/s41586-020-2312-y.

39. Jiang, R.D., Liu, M.Q., Chen, Y., Shan, C., Zhou, Y.W., Shen, X.R., Li, Q., Zhang, L., Zhu, Y., Si, H.R., et al. (2020). Pathogenesis of SARS-CoV-2 in transgenic mice expressing human angiotensin-converting enzyme 2. Cell *182*, 50–58.e8. https://doi.org/10.1016/j.cell.2020.05.027.

40. Netland, J., Meyerholz, D.K., Moore, S., Cassell, M., and Perlman, S. (2008). Severe acute respiratory syndrome coronavirus infection causes neuronal death in the absence of encephalitis in mice transgenic for human ACE2. J. Virol. *82*, 7264–7275. https://doi.org/10.1128/jvi.00737-08.

41. Ziegler, C.G.K., Allon, S.J., Nyquist, S.K., Mbano, I.M., Miao, V.N., Tzouanas, C.N., Cao, Y., Yousif, A.S., Bals, J., Hauser, B.M., et al. (2020). SARS-CoV-2 receptor ACE2 is an interferon-stimulated gene in human Airway epithelial cells and is detected in specific cell subsets across tissues. Cell *181*, 1016–1035.e9. https://doi.org/10.1016/j.cell.2020.04.035.

42. Flodby, P., Li, C., Liu, Y., Wang, H., Rieger, M.E., Minoo, P., Crandall, E.D., Ann, D.K., Borok, Z., and Zhou, B. (2017). Cell-specific expression of aquaporin-5 (Aqp5) in alveolar epithelium is directed by GATA6/Sp1 via histone acetylation. Sci. Rep. *7*, 3473. https://doi.org/10.1038/s41598-017-03152-7.

43. Rock, J.R., Barkauskas, C.E., Cronce, M.J., Xue, Y., Harris, J.R., Liang, J., Noble, P.W., and Hogan, B.L. (2011). Multiple stromal populations contribute to pulmonary fibrosis without evidence for epithelial to mesenchymal transition. Proc. Natl. Acad. Sci. U S A *108*, E1475–E1483. https://doi.org/10.1073/pnas.1117988108.

44. Zou, X., Chen, K., Zou, J., Han, P., Hao, J., and Han, Z. (2020). Single-cell RNA-seq data analysis on the receptor ACE2 expression reveals the potential risk of different human organs vulnerable to 2019-nCoV infection. Front. Med. *14*, 185–192. https://doi.org/10.1007/s11684-020-0754-0.